Functional fatigue of $Ni_{50.3}Ti_{25}Hf_{24.7}$ – Heterogeneities and evolution of local transformation strains

Wael Abuzaid, Huseyin Sehitoglu

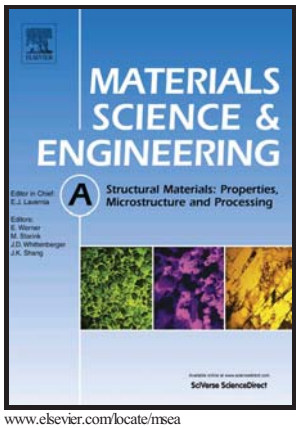

www.elsevier.com/locate/msea

PII: S0921-5093(17)30578-6
DOI: http://dx.doi.org/10.1016/j.msea.2017.04.097
Reference: MSA34998

To appear in: *Materials Science & Engineering A*

Received date: 30 December 2016
Revised date: 24 April 2017
Accepted date: 25 April 2017

Cite this article as: Wael Abuzaid and Huseyin Sehitoglu, Functional fatigue o
$Ni_{50.3}Ti_{25}Hf_{24.7}$ – Heterogeneities and evolution of local transformation strains
Materials Science & Engineering A
http://dx.doi.org/10.1016/j.msea.2017.04.097

Submitted to Materials Science and Engineering: A, December 2016

Revised April 2017

Functional fatigue of $Ni_{50.3}Ti_{25}Hf_{24.7}$ – Heterogeneities and evolution of local transformation strains

Wael Abuzaid [1], Huseyin Sehitoglu [2]

[1] Department of Mechanical Engineering, American University of Sharjah, PO Box 26666, Sharjah, UAE

[2] Department of Mechanical Science and Engineering, University of Illinois at Urbana-Champaign, 1206 W. Green St., Urbana, IL 61801, USA

Abstract:

Shape memory alloys achieve their unique and desirable property of large recoverable strains through phase transformation. The attained magnitudes of transformation strains is strongly affected by the level of deformation heterogeneity during the transformation process and is impacted by plastic deformation and the accumulation of retained martensite/austenite following repeated cycling. This paper is dedicated to study the heterogeneity in the total and transformation strains of the high temperature shape memory alloy $Ni_{50.3}Ti_{25}Hf_{24.7}$ subjected to fatigue loading and aims to provide further insight to the source of transformation strain instability. Under isobaric loading conditions, full field strain measurements were collected during thermal cycling and utilized to assess the local changes in the deformation field. Transformation strains increased globally in the first few cycles of loading followed by a relatively stable response and eventually started to exhibit drop in their magnitudes with continued loading. No homogenization of the transformation strain field was observed as a result of either stress increase or thermal cycling. The transformation strains were localized and the global evolution in their magnitudes was associated with local changes, either increasing or decreasing local strains, in spatially the same regions. The experimental results are discussed with the aim to provide a deeper understanding of the stability of transformations strains, their

evolution under cyclic loading, the heterogeneities developing in the deformation field, and the relation between local and global response due to the accumulation of irrecoverable strains.

Keywords: Transformation strain, High temperature shape memory alloy, NiTiHf, Functional fatigue, Digital image correlation, Plastic stra

1. Introduction:

One of the most promising candidates for high temperature shape memory alloys (SMA) is NiTiHf [1-3]. The addition of Hf results in an increase in transformation temperatures (TTs) thus allowing applications that are otherwise not possible using traditional NiTi SMAs which can only operate below 100 ºC [3, 4]. Many studies have demonstrated shape memory properties and TTs in the range of 100 – 300 ºC [5-12] and a remarkable 400 ºC range for the Hf rich compositions[1]. Among other factors (*e.g.,* heat treatment [9, 13-17]), Hf content significantly affects the properties of the SMA and the resulting TTs. To date, Hf 25 at.% has shown the best combination of properties in terms of operating at high TTs, high strength and large transformation strains compared to the lower Hf content compositions [1]. Most of the available experimental works, however, have been focused on a single or a few loading cycles (*e.g.,* single or few temperature cycles in an isobaric constant stress loading conditions). One aspect that needs further investigation is the functional properties of the alloy under fatigue loading conditions. A better understanding of the evolution of shape memory properties (*e.g.,* transformation strain) under fatigue is crucial for the implementation of this class of alloys in critical applications [18].

The importance of experimental analysis under fatigue loading conditions becomes extremely important when studying the stability of the SMA over a large number of cycles [18, 19]. Although measurements from a single or few cycles can provide insight into transformation temperatures, transformations strains, and plastic or irrecoverable deformation, the evolution of these magnitudes can be significant and taking place at a relatively fast rate, particularly in the first few cycles. For example, Kockar *et al.* have shown an evolution in the transformation strains over 10 temperature cycles in an isobaric experiment conducted on NiTi8Hf SMA [19]. These changes were associated with plastic deformation resulting in cyclic instability and an increase in total strains. The work of Sedmak *et al.* provides another example where Synchrotron X-ray diffraction was used to reveal, in superelastic cyclic experiments on NiTi SMA, changes in the defect density, lattice strains and consequently residual stress, and the residual volume fraction of austenite and martensite [20]. These changes at the microstructural level have a significant influence on the shape memory properties of the SMA. The exact steps leading to the instability in transformation strains is still under debate. However, the accumulation of plastic strains and/or residual martensite during cycling are known to impact the functional response and result in transformation strain deterioration. The accumulation of residual martensite (or austenite) can be captured using neutron diffraction experiments. This work emphases is on providing a clear and detailed assessment of the correlation between plastic strain accumulation (which can't be measured using Synchrotron X-ray diffraction) and its impact on transformation strains over the life of the SMA. We utilized digital image correlation (DIC) to collect full field strain measurements of the transformation strains (local measurements) and monitor local changes in the transformation strain field under isobaric, thermal cycling loading conditions. The evolution of irrecoverable plastic strains was analyzed and used to provide further insight into

the local changes in the transformation strains (beyond 10 cycles, 50 cycles – failure in tension). Also, and to better understand the role of global/local stress, experiments with incremental increase in stress were conducted. The increase in stress can alter the local defect density and the local stresses in the SMA. As will be shown in this paper, the changes introduced by global stress increase significantly alters the accumulation of plastic strains and consequently the local transformation strains and their evolution in fatigue.

In previous experimental works on NiTi and NiTiHf, the deviation between the experimentally measured transformation strains and the theoretical expected values based on lattice deformation theory (LDT) was discussed, *e.g.,* [8, 21]. For example, an average transformation strain of about 8 % was reported previously for NiTiHf single crystal samples loaded along the $[111]_{B2}$ direction compared to an expected 18.9 % based on LDT theoretical calculations [22]. In general, this discrepancy between theoretical calculations and the observed experimental results has been attributed to local regions not contributing to the transformation (*i.e.,* heterogeneous deformation). As the theoretical calculations are based on a single crystal of austenite transforming to a single crystal of martensite, any non-transforming regions will impact and decrease the measured transformation strains. Patriarca *et al.* have observed through high temperature X-Ray diffraction the presence of residual martensite above the austenite finish temperature A_f [22]. Sedmak *et al.* [20] made similar observations using neutron diffraction. Another source, as discussed by Stebner *et al.*, is the presence of precipitates in the matrix which will not contribute to the transformation process [8]. These previous works provide valuable insight into the source of mismatch between experiment and theory. However, the degree of heterogeneity in the transformation strains, which is the source of the observed mismatch, has not been fully assessed. Also, the evolution of the transformation strains, and the level of

heterogeneity, under fatigue loading conditions (functional fatigue) is not well characterized. For example, it's not very clear how the local strains evolve with continued cycling and whether the transformation homogenizes or becomes more heterogeneous. In addition, the impact of localized plastic strains on the heterogeneity of deformation and the evolution of transformation strains is not well understood quantitatively. In this work, we used DIC to collect full field strain measurement during isobaric temperature cycling. The collected full field strain measurements allow for detailed statistical assessment of the degree of deformation heterogeneity, and its evolution, with temperature cycling (functional fatigue). With the availability of full field data, the level of deformation heterogeneity can be visually observed through the strain contour plots or quantitatively by calculating the deformation field standard deviation. The local changes in the deformation field impacting the level of heterogeneity can also be captured (*e.g.,* accumulation of plastic strains and changes in the transformation strains) and used to explain the observed changes in deformation heterogeneity. For example, if an increase in transformation strains is triggered by new regions starting to contribute to transformation, this can be captured using DIC and will be manifested as a homogenization process (*i.e.,* drop in standard deviation and local spreading of high strains). Alternatively, if the instability in the transformation strains is induced by local changes in the stress field (*e.g.,* due to increase in defect density or relaxation induced by plastic deformation), then DIC will portray a significantly different response. In such a case, the strain field will essentially experience variations in the same spatial regions and can be detected using DIC (*i.e.,* local increase or decrease in local transformation strains magnitude). Such analysis is advantageous as it provides quantitative insight into the heterogeneous transformation of SMAs (which is the main cause for deviation between theoretical and

experimentally measured transformation strains), and helps pinpoint the source of these heterogeneities that eventually lead to instabilities in the transformation strains.

In summary, this experimental study is dedicated to explore the functional stability of $Ni_{50.3}Ti_{25}Hf_{24.7}$ SMA. We particularly address the accumulation of irrecoverable plastic strains and study their impact on local transformation strains measured during thermal cycling under isobaric loading conditions. The strain measurements were collected using DIC to provide full field data allowing for the assessment of not only the global response but also the local changes in the transformations strains. We quantify the changes in the transformation strains and provide detailed analysis to pinpoint the source of these changes. The full field data was also used to provide statistical assessment of the heterogeneity developing during martensitic transformation, which is one of the main reasons for the experimentally observed difference in the measured transformation strains and the theoretically expected magnitudes, and how it evolves in fatigue and responds to incremental stress increase. The material selected for this work is the high temperature ternary $Ni_{50.3}Ti_{25}Hf_{24.7}$ (at. %) due to superior properties in terms of high transformation strains, high strength, and high transformation temperatures. To eliminate any effect from grain boundaries or texture, single crystals were utilized. Also, as the transformation strains are orientation dependent, all the reported experiments were conducted on a single orientation (*i.e.,* <111>) tensile samples.

2. Materials and Methods:

Single crystal ingot of $Ni_{50.3}Ti_{25}Hf_{24.7}$ was grown using the Bridgman technique in He atmosphere. Dogbone tension samples (1.5 mm × 3 mm gauge section) were electric discharge machined from the ingot with the loading axis along the $[111]_{B2}$ direction as detailed in [22]. All samples were tested in the homogenized state (1050 ºC for 20 h) having the following

transformation temperatures; austenite start temperature A_s = 251 °C, austenite finish temperature A_f = 422 °C, martensite start temperature M_s = 340 °C, and martensite finish temperature M_f = 214 °C. Such high temperatures far exceed the TTs reported in early works on lower Hf compositions [13] and opens new potential applications. Based on diffraction, the austenite and martensite phases were determined as B2 and B19′ respectively.

Prior to loading, samples were polished using SiC paper up to P1200 to remove any surface scratches. The speckle pattern for DIC measurements was applied using very high temperature black paint that can withstand temperatures greater than 1000 ºC. The quality and stability of the pattern was suitable for the temperatures considered (up to 450 ºC) and span of experiments (up to 285 cycles). The back surface of the sample was also painted with a high temperature black paint to allow for temperature measurements and control using an IR thermometer focused on the center of the gauge area. Isobaric thermal cycling experiments were conducted using an Instron servo hydraulic load frame and a Lepel induction heating system. Temperature control was achieved using a Micristar temperature controller. DIC reference images were captured at the maximum temperature (450 ºC) and no load. A total of 5 images were captured to cover the entire gauge section of the sample with an imaging resolution of ~ 2.04 μm/pixel. In the first temperature cycle, deformed images covering the entire section were also captured after loading to the desired stress level followed by cooling to the minimum cycle temperature (190 ºC) to induce austenite to martensite phase transformation. Subsequent image collection (beyond the first cycle) was based on a single image (1600 × 1200 pixels) covering an area of approximately 3.2 mm × 2.4 mm and collected every 10s during thermal cycling. A typical cycle was 16 minutes; 7 minutes cooling from 450 to 190 ºC (in air), a one minute hold at 190 ºC, 7 minutes heating to 450 ºC, and a 1 minute hold at 450 ºC before repeating the cycle (cooling). DIC

correlations with reference to the original image at 450 ºC under no load are measurements of total strain which includes transformation strains and any irrecoverable components. Correlations conducted between images collected at the beginning of a cooling cycle (*i.e.*, 450 ºC, loaded) and the end of the same cycle (*i.e.*, 190 ºC, loaded) focus predominantly on the transformation component of the strain and is not affected by any prior accumulation of irrecoverable strains.

The different measurements and parameters collected and analyzed in this work are graphically explained in Fig. 1. Each point in the Strain – Temperature plot (Fig. 1a) was generated from the DIC field average (*i.e.*, mean strain from DIC) and the corresponding temperature at the same time the associated deformed image was captured. A typical contour plot showing the variation and heterogeneity in strain field is shown in Fig. 1b. The full field data can also be summarized and represented in the form of a strain histogram (strain distribution) as shown Fig. 1c. Calculating the standard deviation from the full field data (or the strain histogram) provides a clear assessment of the level of deformation heterogeneity in the area of interest.

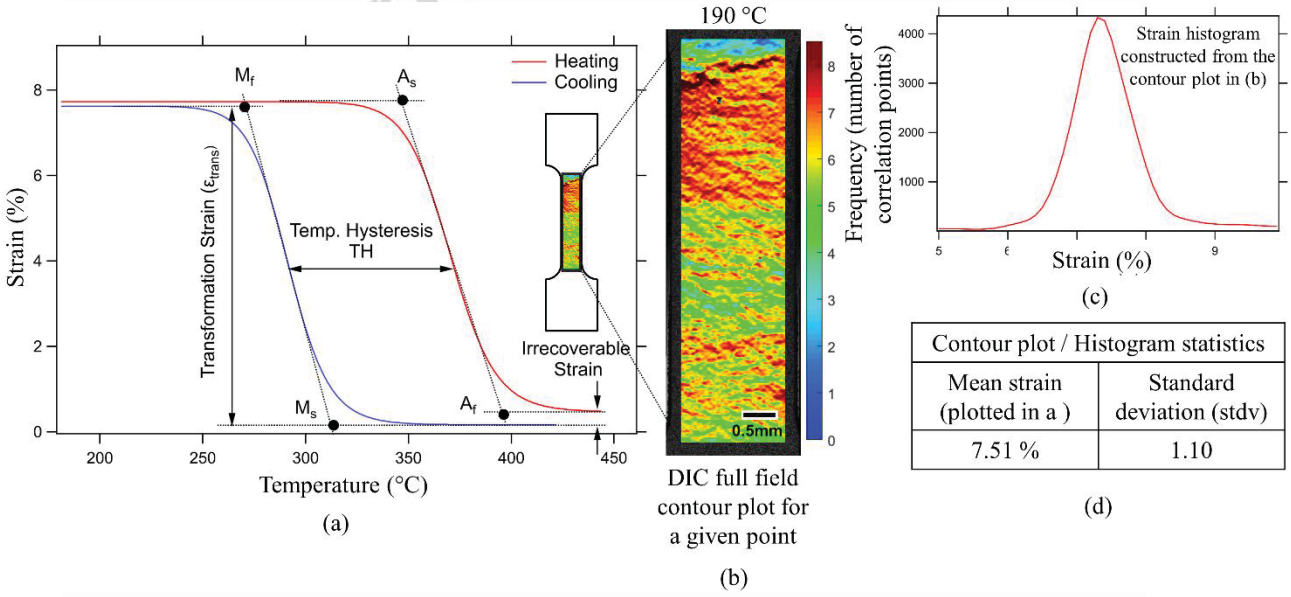

Contour plot / Histogram statistics	
Mean strain (plotted in a)	Standard deviation (stdv)
7.51 %	1.10

(d)

Fig. 1. Schematic detailing all the transformation specific properties extracted from an isobaric, constant stress, thermal cycling experiment. Each point plotted in (a) represents the field average (mean strain) obtained from DIC contour plots as shown in (b). Strain histogram (c) and mean and standard deviation can be calculated for each DIC contour plot as shown in (d).

3. Results and Analysis

The strain-temperature behavior of a sample subjected to 250 MPa tensile stress and a single temperature cycle is presented in Fig. 2a. The solid line curve was generated from DIC field averages over a large area covered by a single reference and deformed images (global region). The dashed line was generated from a smaller region with localized transformation strains and represents the local response rather than the global response. The corresponding contour plot in Fig. 2b shows the heterogeneity and localizations in the transformation strains field. The variation between global, macroscopic, strains and local magnitudes is manifested in the contour plot and the two strain-temperature curves generated from a global region and a local high strain region (both marked on the contour plot in Fig. 2b).

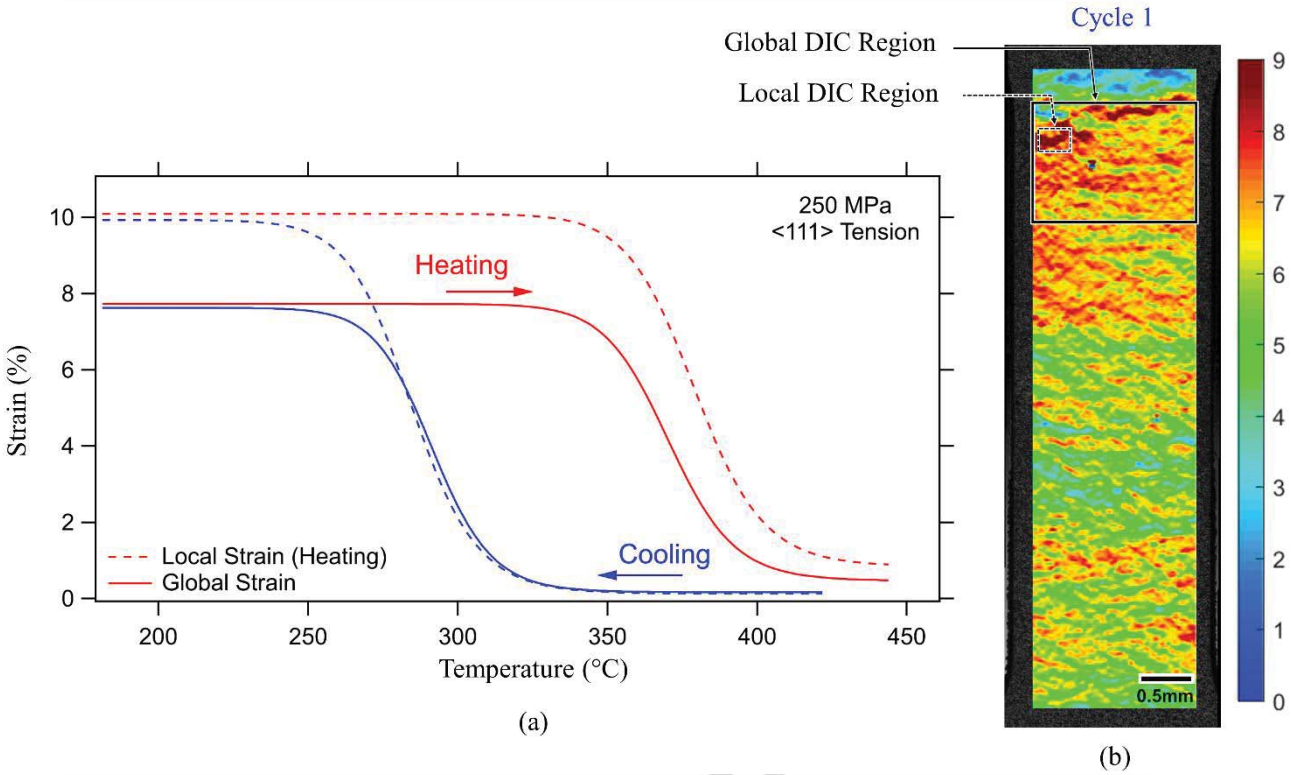

Fig. 2. (a) Strain – temperature response for a <111> single crystal of $Ni_{50.3}Ti_{25}Hf_{24.7}$ showing a comparison between global (solid line) and local (dashed line) strains. The contour plot in (b) was generated from 5 DIC images stitched together to cover the entire gauge section of the sample. The global strain-temperature plot in (a) was generated using a single image region, marked as "Global DIC Region" in (b). The local data was extracted from the high strain region marked as "Local DIC Region" in (b).

The strain-temperature behavior of a sample subjected to 200 MPa tensile stress and 50 temperature cycles is shown in Fig. 3 (selected cycles for improved clarity). The inset in Fig. 3a provides an enlarged view focusing on the maximum measured total strain at the end of the cooling cycle (*i.e.*, 190 ºC at end of austenite – martensite transformation). The total measured strains at this point increase with cycle number with larger increments taking place in the first few cycles followed by a slower rate of increase towards higher cycle numbers. Selected contour plots covering the entire gauge section of the sample are shown in Figs. 3b-3c and provide evidence of an increased levels of local strains (notice the darker red regions in (c) compared to (b)). The increase and accumulation of irrecoverable strain with cycle loading can be observed

also in Fig. 3a. The total strains reported in Fig. 3 includes transformation strains and any irrecoverable accumulated strains.

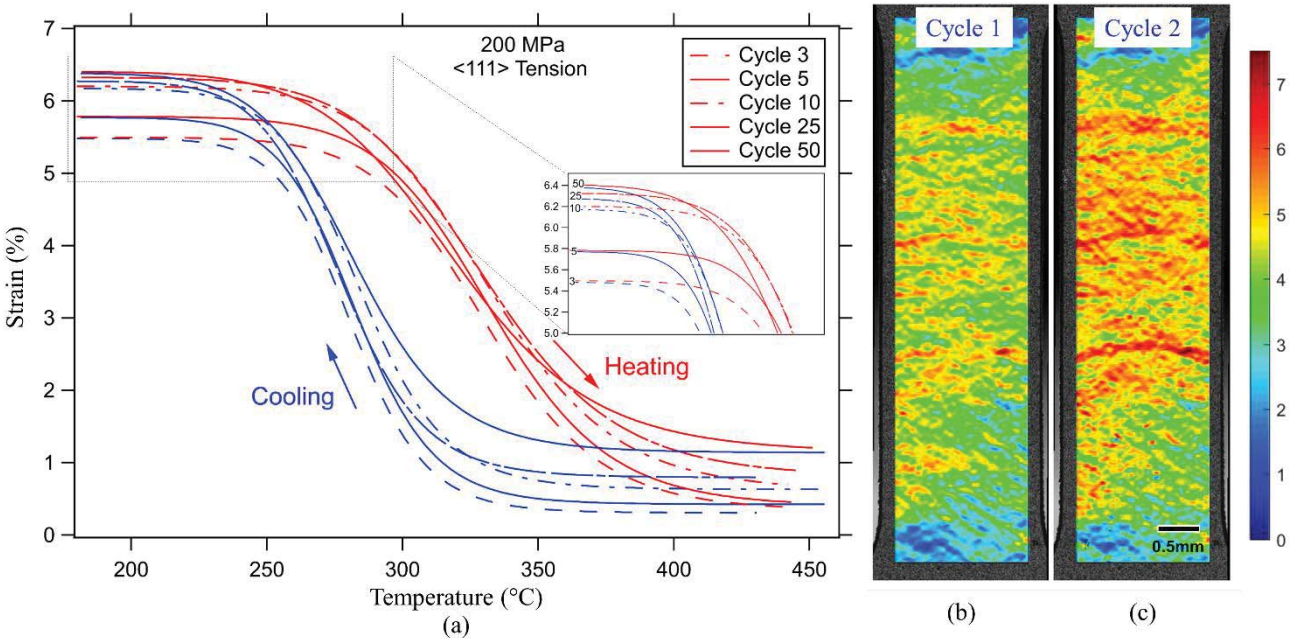

Fig. 3. (a) Strain – temperature response for a <111> single crystal of $Ni_{50.3}Ti_{25}Hf_{24.7}$ loaded at a constant stress of 200 MPa and subjected to 50 temperature cycles. The contour plots for the first 2 cycles are presented in (b) and (c) and show a clear increase in local strains for the second cycle. A clear increase in the total strain is observed in the first few cycles. The rate of increase slows down with continued loading. Accumulation of irrecoverable strains is also observed with continued loading (*i.e.*, increase in the total strains measured at 450 °C)

As the focus in this work is on transformation strains, additional correlations were conducted within each cycle (*i.e.,* reference image at 450 ºC and deformed image at the end of the cooling cycle at 190 ºC as explained in Section 2. and Fig. 1). Such procedure allows for the isolation of the transformation strain component from the total strain that includes, in addition to transformation strains, the irrecoverable strains which are observed to accumulate with cycle number. The evolution of transformation strains with cycle number is shown in Fig. 4a for the three different stress levels (150, 200, and 250 MPa), all subjected to similar temperature cycling between 190 to 450 ºC. In general, the transformation strain increase in the first few cycles, followed by a saturation region where their magnitude appears to be stable, and finally a third

region where they experience a drop in magnitude with continued loading. The span of the first two regions is very dependent on the stress level and decrease with increasing stress level (notice that the number of cycles before transformation strains start to drop is less for the 250 MPa case compared to the 200 and 150 MPa samples). Another important aspect noticed in Fig. 4a is the rate at which the transformation strains drop (3rd region); at the highest considered stress level (250 MPa), the transformation strains shows a sharp and continuous degradation with cycle number. The rate of decrease is significantly less at 200 MPa and almost insignificant at 150 MPa and can only be observed at relatively much larger cycle number (exceeding 250 cycles) as shown in Fig. 4b.

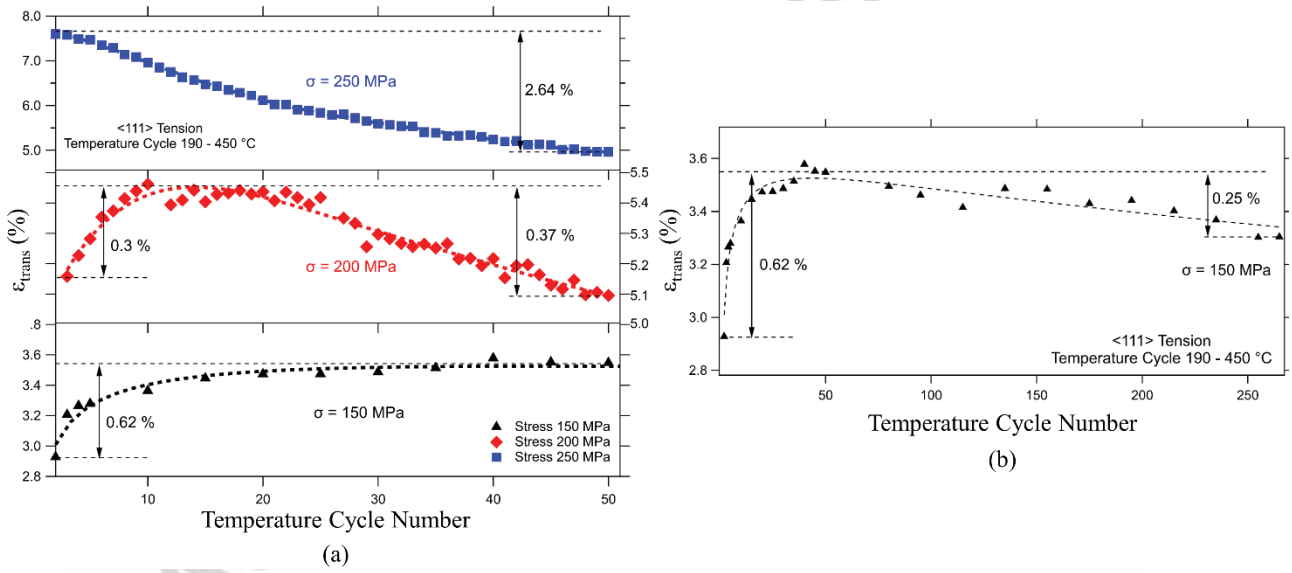

Fig. 4. (a) The evolution of transformation strains with cycle number (50 cycles) for samples subjected to isobaric thermal cycling loading conditions, three sample with three different stress levels. A drop in transformation strains was not observed in the first 50 cycles at 150 MPa, however a slight decrease becomes visible beyond 100 cycles as shown in (b) for the same stress level.

To further investigate the correlation between the global applied stress and the transformation strain evolution, an isobaric experiment was conducted with incremental stress increase after 15 temperature cycles at each stress level starting from 150 MPa to 250 MPa on

the same sample. The loading conditions are detailed in Fig. 5 while the strain-temperature for selected cycles at each stress level are shown in Fig. 6. The total strains increase with cycle number and every time the global stress is increased. The accumulation of irrecoverable strains with cycle number is insignificant at 150 MPa, increases slightly at 200 MPa, and experiences significant accumulation once the stress is raised to 250 MPa. For increased clarity, the first cycle at each stress level is plotted on a single figure (Fig. 6d). Besides the significant increase in total strain with stress increase, an increase in TH is observed along with an increase in the A_s temperature.

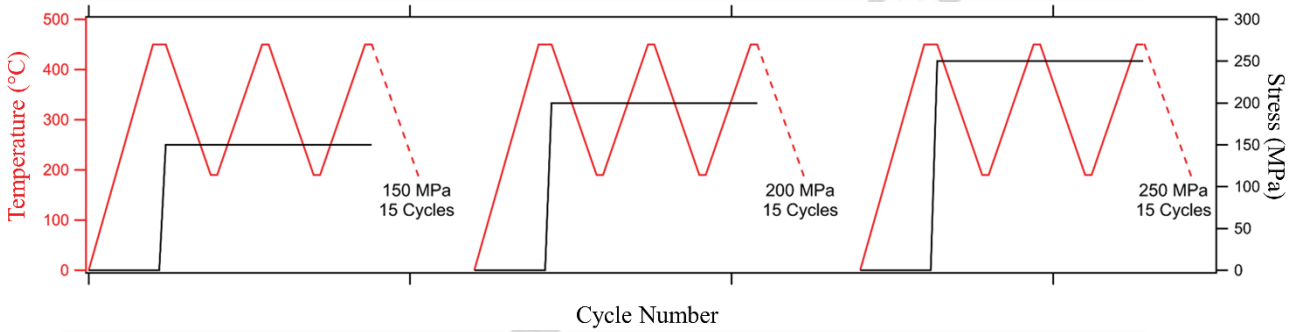

Fig. 5. Loading conditions for the incremental stress loading experiment. The same sample was loaded for 15 temperature cycles at the each particular stress level.

The transformation strain (not the total strain) contour plots for first cycle at each stress level are shown in Fig. 7 for the entire gauge section. An increase in the local transformation strain magnitudes is observed. This increase appears to take place in the same spatial regions. Some regions with very small, or no contribution to the transformation strain (*i.e.*, the blue regions in the contour plots) are persistent and do not change the transformation strains once the stress is increased. The corresponding strain histograms are shown in Fig. 7d and shows widening of the histogram that can be associated with an increased level of deformation

heterogeneity developing in the material (notice the increase in the standard deviation). Cycle – cycle analysis is presented in Fig. 8

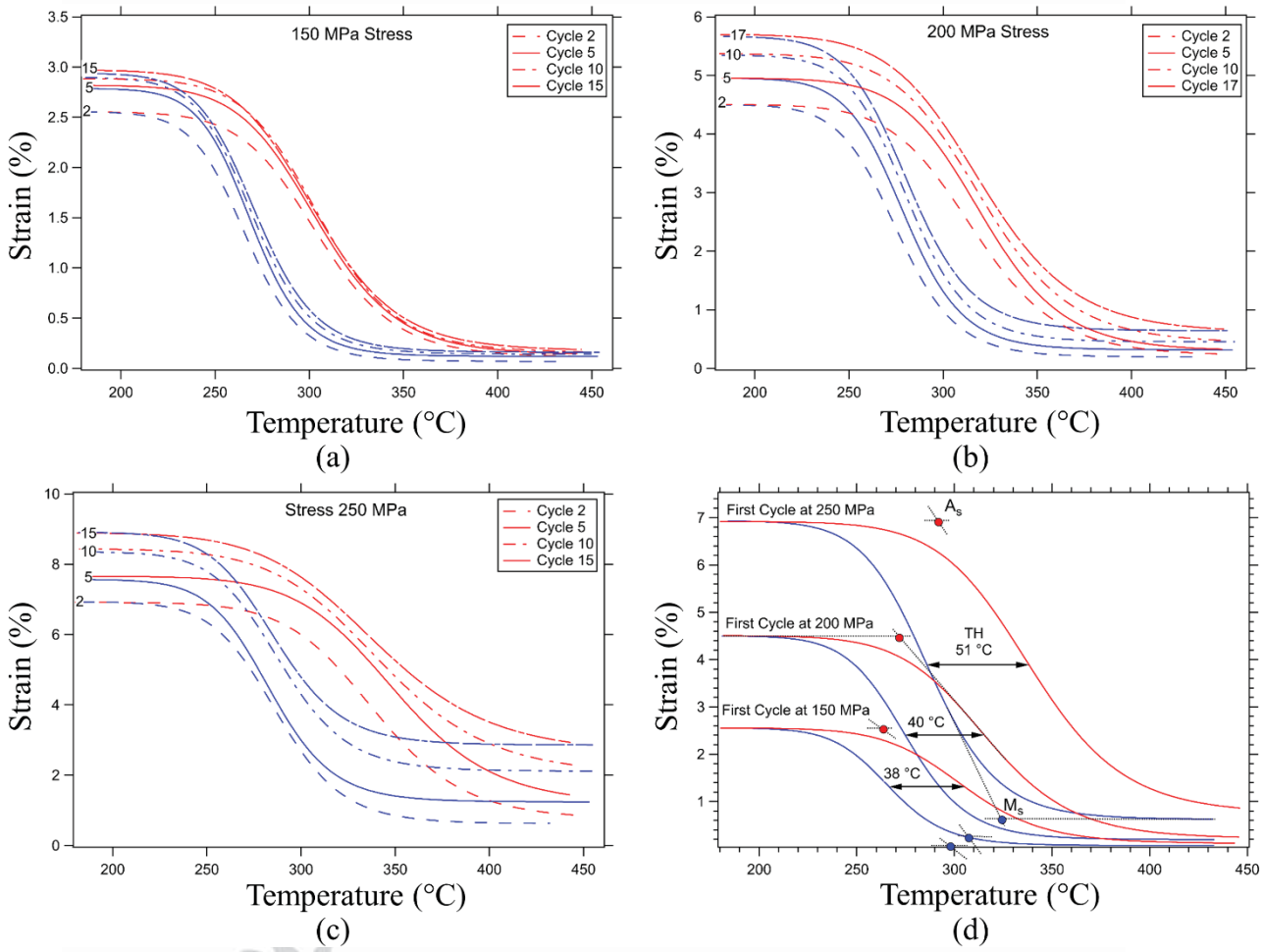

Fig. 6. (a) – (c) Strain – temperature response for a <111> single crystal of $Ni_{50.3}Ti_{25}Hf_{24.7}$ loaded incrementally as shown in Fig. 5. (d) A comparison between the first cycle at each stress level showing a clear increase in A_s temperature and temperature hysteresis TH with increasing stress level.

To better understand the cycle-cycle changes taking place during thermal cycling and the disruption introduced by global stress increase, the evolution of the transformation strains is presented for the entire experiment (a global region of ~ 2.8 × 1.8 mm as captured using a single image) in Fig. 8a. The transformation strain at 150 MPa, similar to what was observed in separate experiments in Fig. 4, increased in the first few cycles followed by a saturation region.

The incremental increase in transformation strain was resumed, and triggered, by the global stress increase to 200 MPa. The last 2 point at 200 MPa showed no change indicating that the saturation region was reached. The final stress increase to 250 MPa triggered transformation strain increase another time but was followed by a very short saturation region and eventually a drop in transformation strains with continued cycling. In the cases where a transformation strain increases was observed within the first few cycles at each stress level, a corresponding increase in the DIC transformation strain field standard deviation was measured as shown in Fig. 8b. The regions where saturation was more prevalent, the transformation strain experienced very little fluctuations.

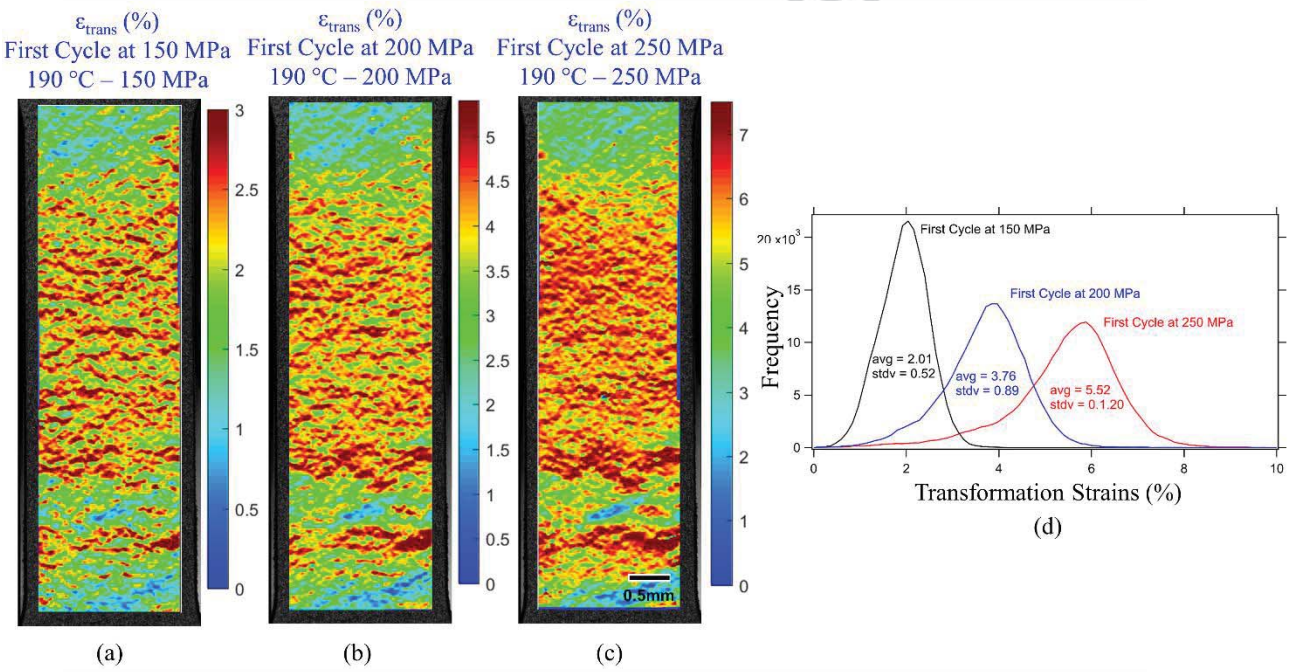

Fig. 7. (a) – (c) Contour plots of the transformation strains for the first cycle at each stress level shown in Figs. 5-6. By adjusting the scale bars at each stress level, it becomes clear that the total increase in transformation strains is accomplished by strain accumulation in the same local regions (notice the similarity in the localization regions for the contour plots). The corresponding strain histograms are presented in (d) and shows an increased level of deformation heterogeneity (*i.e.,* larger Stdv and widening of the strain histogram) with stress increase.

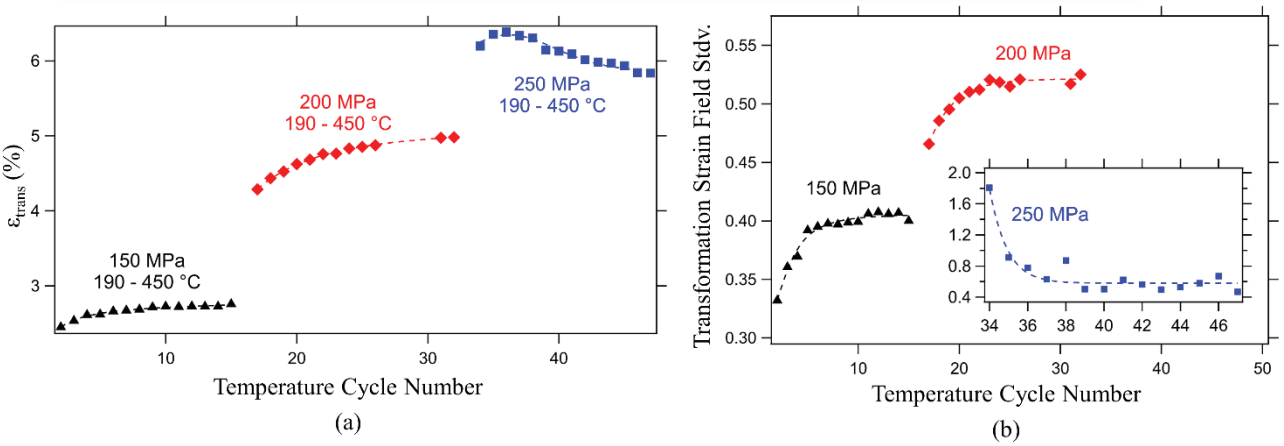

Fig. 8. (a) Evolution of mean (DIC contour plot field average) transformation strains and DIC field standard deviation (b) with cycle number for the three different stress levels shown in Figs. 5 and 6.

To further elaborate on the local changes in the transformation strain field leading to changes in the standard deviation and an increased level of deformation heterogeneity in the first few cycles (*i.e.*, regions where an increase in the transformation strain was observed), we focus on the 150 MPa. This stress level was selected as it did not show any decrease in the transformation strains during the considered number of cycles. Strain histograms for selected cycles are presented in Fig. 9b and show the initial increase in strain followed by saturation. The line scan analysis (drawn on the contour plot in Fig. 9a) shows that the transformation strains clearly and predominantly accumulated in the same regions while low strain regions experienced insignificant change during continued thermal cycling. The contour plots for a selected region (also marked in Fig. 9a) supports the line scan analysis and clearly shows a local increase in the transformation strains.

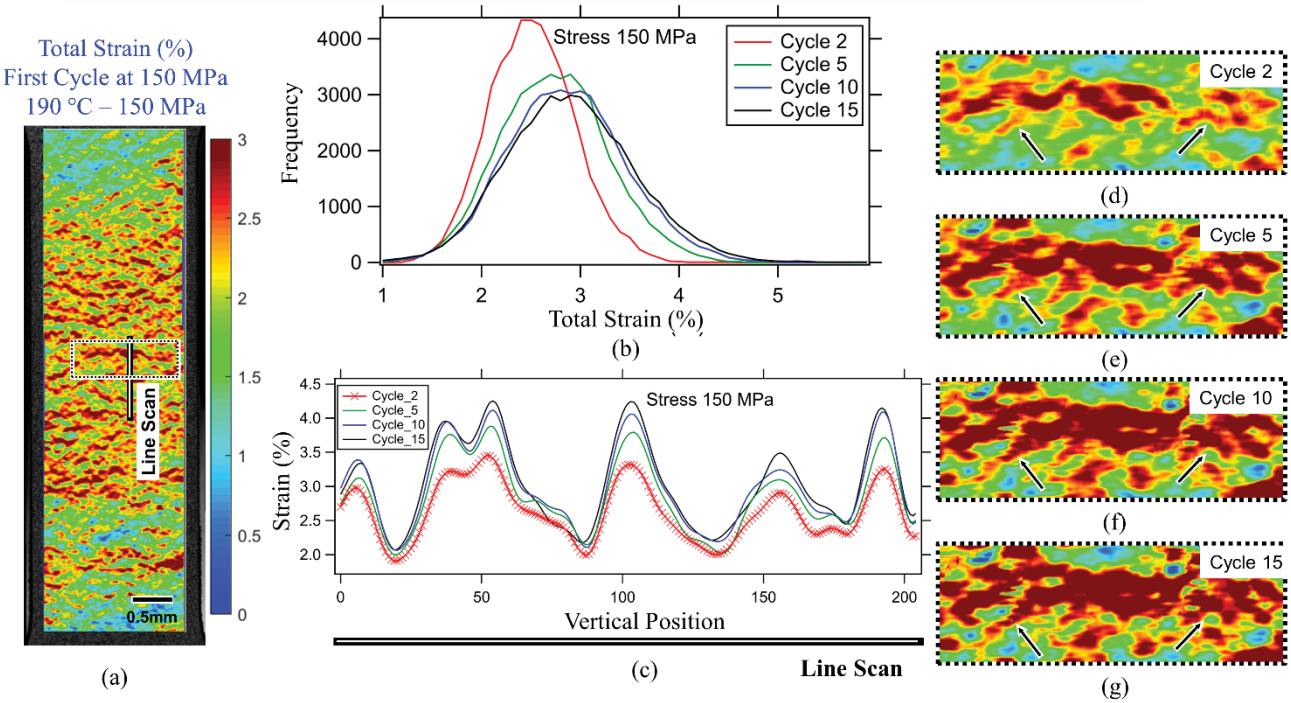

Fig. 9. (a) Contour plot of the first cycle total strain at the 150 MPa stress level for the incremental experiment described in Fig.5. An increase in the total strain (which is equal to transformation strain in this case) is shown in the strain histograms presented in (b). (c) Shows line scan, marked in (a), results indicating that the initial increase in strains takes place in the same spatial regions. Contour plots (d) – (e) shows the evolution of strain and an increased level of strain accumulation in the first few cycles.

The other important aspect under investigation in this work is the drop in the transformation strains with continued thermal loading (see Figs. 4 and 8). The extreme case of 250 MPa stress, which clearly shows the drop and decline in the magnitude of transformation strains was selected for this analysis. Figure 10a shows histograms of the total strains (includes transformation and irrecoverable strains). A shift in the histograms was observed with mean, minimum (associated with irrecoverable accumulated strains), and maximum strains all increasing. To shed further insight into the source of this shift in strains (*i.e.*, is the change induced by changes in the transformations strains or the irrecoverable strain component), strain histograms of the transformation strains *only* were constructed (Fig. 10b). A summary of the total and transformation strain evolution with cycle number is presented in Fig. 10c. The change in the

total strains over the 15 cycles considered at 250 MPa was about 2% increase while the transformation strains experienced a decrease of about 0.4 % over the considered number of cycles. The contour plots presented in Figs. 10d – 10g provides examples of local regions that experience a degradation in the transformation strains with cycling which is consistent with the global/average results shown in the Figs. 10b -10c.

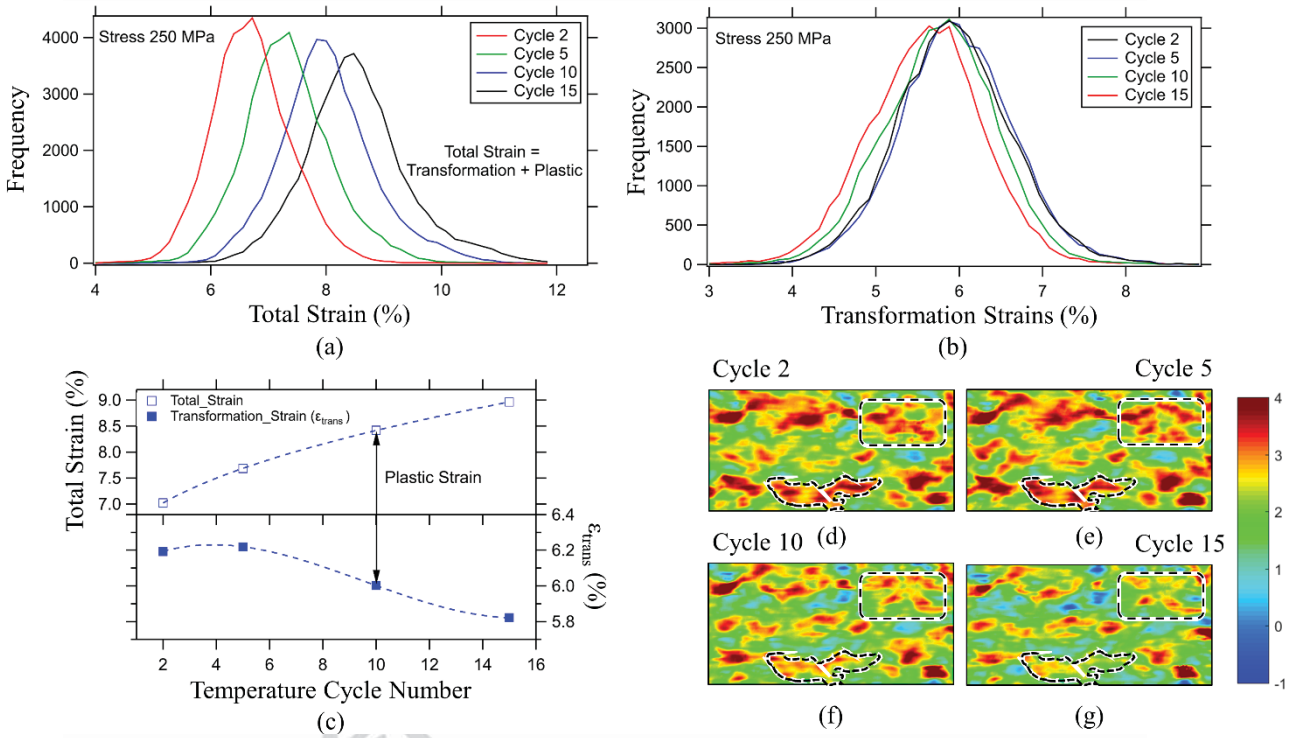

Fig. 10. (a) Strain histograms for the total strains measured during the incremental experiment described in Fig.5 at the 250 MPa stress level. A clear increase in the total strains is observed. (b) Strain histograms for the transformation strain only. (c) Mean strain evolution for the histograms shown in (a) and (b), note that although the total strain increases with continued loading, the transformation strains actually experience reduction. (d) – (g) Contour plot of the transformation strain for select cycles showing local decrease in strain (notice the 2 marked regions).

At the end of the incremental experiment (*i.e.*, the 15 cycles at each stress level) and after observing a relatively large drop in transformation strains accompanied with continued accumulation of irrecoverable strains at the highest stress, 250 MPa, the question of whether dropping the stress below 250 MPa will stop the degradation in transformation strains arises. To

address this question, 3 additional cycles at each stress level were applied to the same sample and the transformation strains were measured. The measured transformation strains for each cycle and stress level are presented in Fig. 11. After dropping the stress level to 150 MPa, the transformation strains were constant through the 3 cycles. The incremental decline in transformation strain was resumed once the stress level was increased back to 250 MPa.

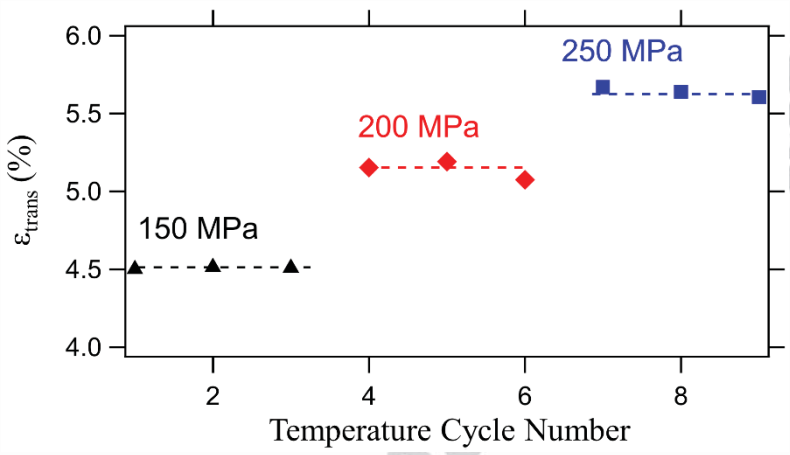

Fig. 11. The evolution of the transformation strains under isobaric temperature cycling loading condition, 3 stress levels and 3 cycles at each stress level. The results represent additional loading for the same sample presented in Figs. 5 – 10.

4. Discussion

4.1. Local and Global Transformation Strain Measurements

The work presented in this paper was focused on providing further insight into the functional fatigue properties of the high temperature $Ni_{50.3}Ti_{25}Hf_{24.7}$ SMA. The utilization of DIC to collect full field strain measurements has been crucial in highlighting the heterogeneity developed in the material during transformation and how it evolved when subjected to temperature cycling. For example, the contour plots shown in Fig. 2 shows a clear level of deformation heterogeneity with strain localizations in the transformation strain field. This heterogeneity, and the fact that some regions are clearly not contributing to the transformation process (notice the blue regions in Fig.

2) is one source why the global measured transformation strains will in general be lower than what is expected by theory. The local strains, however, are in closer agreement with theory and should be a fundamental quantity to consider when studying the transformation capacity of SMAs. Although DIC can highlight this variation between local and global measurements and clearly delineate domains that do not contribute to the transformation process, the reason behind this response remains unanswered. Further analysis will be required to highlight possible causes. In previous work by Patriarca *et al.* [22] using the same material considered in this study, high temperature X-ray diffraction revealed the presence of residual martensite above A_f. Obviously these regions will not contribute to the transformation process during the cooling cycle and will results in the non-transforming regions observed in the DIC strains field. Another source observed in this work is the presence of large Hf rich inclusion in the material as shown in the SEM micrograph with corresponding EDX analysis in Fig. 12. These inclusions will not transform during temperature cycling. Eliminating these inclusions will potentially help in reducing the level of deformation heterogeneity and result in an increase in the global transformation strain (obtained from DIC field average). We note that full field analysis, as conducted in this paper using DIC, provides adequate means for capturing the localizations introduced by these microstructural features and will be a proper tool to assess and compare any changes affecting the presence of these inclusions and thus the resulting transformation strains. We finally note that the conducted measurements are limited to the surface of the material and lacks full assessment of subsurface effects. This limitation, which is common in all surface measurement techniques, is not expected to have a major impact on the conclusions made in this work as single crystal samples were considered.

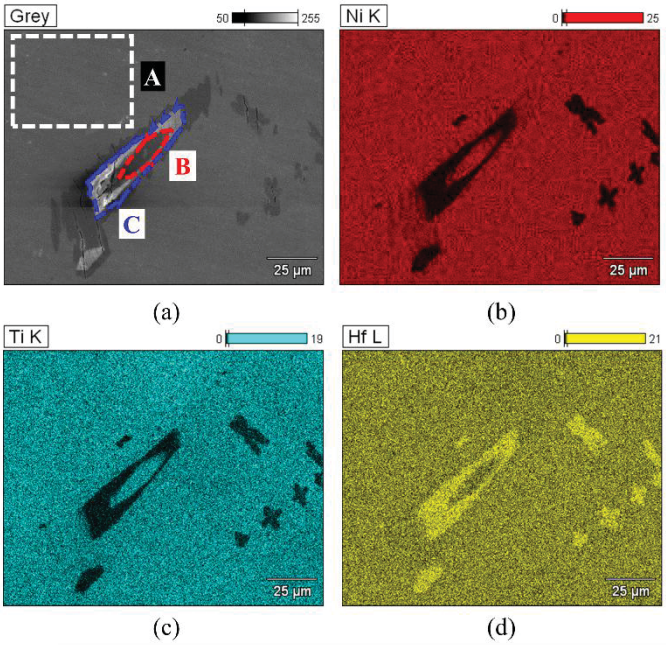

EDX Analysis for regions marked in (a)

Location	Ni Atom %	Ti Atom %	Hf Atom %
A	51.78	21.53	26.69
B	48.06	21.20	30.74
C	13.86	5.51	80.63

(e)

Fig. 12. (a) SEM micrograph showing a typical inclusion observed in the SMA considered in this study. Notice the small cracks developing within and around the inclusion. (b) – (d) EDX maps for alloy constituents. Quantitative elemental analysis for the three regions marked in (a) is presented in (e).

4.2. The Evolution of Total and Residual Strains – Potential Role of Plasticity

The strain – temperature response curves for 50 cycles (Fig. 3) shows an increase in both the total and the residual irrecoverable strains with temperature cycling. Similar instability in the material response has been observed by other researchers. For example, Kockar *et al.* have made similar observations on the total strains and have attributed the instability to plastic deformation via dislocation slip [19]. However, as the total strain includes both transformation and irrecoverable, it's important to isolate the transformation strains (ε_{trans}) to better understand if the observed changes in total strains are dominated by the accumulation of irrecoverable strains or changes in the transformation strains field. For instance, despite the fact that the total strains increase with temperature cycling, the analysis of the transformation strain evolution (Fig. 4) has revealed different stages in their response with an obvious stress dependence. In general, the transformation strains increase initially, then stabilize, and eventually start to decrease with

continued loading. The rates of ε_{trans} increase and decrease is strongly affected by stress level, for example, a drop of about 0.4 % in ε_{trans} was observed for the 200 MPa isobaric experiment over 50 temperature cycles while that magnitude increased to 2.6 % for the 250 MPa experiment over the same number of cycles. Lowering the stress further to 150 MPa resulted in a much slower rate of drop with a total decrease of 0.25% over 285 cycles. The correlation between increasing the stress level and the rate of ε_{trans} drop suggest that plastic deformation may be the source of such response. The incremental experiment discussed in Fig. 6, which was conducted on a single sample, thus eliminating any sample dependence effects, provides additional insight into this question of why the transformation strains drop with temperature cycling. By incrementally increasing the stress level on the same sample, the level of accumulated irrecoverable strains clearly increased. In addition, the increase in temperature hysteresis as observed in the first cycle at each stress level also suggests the accumulation of plastic strains[23].

Although the previous observations highlights the correlation between the accumulation of irrecoverable strains and the drop in transformation strains, it is not clear yet how the accumulation of irrecoverable strains induces a drop in transformation strains. Also, the question of why the transformation strains increase in the first few cycles remains unanswered. The local measurements of the transformation strains were utilized to provide further insight into these issues. To address the first questions (*i.e.,* why do ε_{trans} drop), we focus on the results presented in Fig. 10 which were collected at 250 MPa. The largest drop in transformation strains was observed at this stress level. The strain histograms and the corresponding summary data in Fig. 10c shows an increase of about 2% in the total strains accompanied by a drop of only 0.4 % in ε_{trans} over 15 temperature cycles. The contour plots in Fig. 10d – 10g delineates the regions where the drop in ε_{trans} occurred (notice the marked regions). In the two marked regions, a clear

drop in the local level of ε_{trans} was measured using DIC (regions going from dark red at cycle 2 to green at cycle 15). The reason behind why these local regions seized to contribute, or experienced a drop in transformation strains, can be either local stress relaxation due to plasticity or the accumulation of retained austenite or martensite in the transforming regions so that they stop contributing to the transformation during further temperate cycling. From a DIC perspective both of these will appear the same as a local decrease in transformation strains. However, if the accumulation of retained martensite was the sole source behind the drop in transformation strains, then the total increase in irrecoverable strains would have been equal to the total drop in transformation strains (given the fact that no major redistribution of the transformation strains was observed as discussed in Fig. 7). This is however not the case in the observed results which suggest a major role for plastic deformation relaxing the local stress field and leading to incremental drop in the local transformation strains as observed in the contour plots in Fig. 10. Although local stress measurements was not available in this work, other relevant studies in the literature have collected local stress measurements in SMAs subjected to cyclic loading. For example, Sedmak *et al.* used neutron diffraction experiments and reported a drop in the lattice strains, and consequently a drop in local stresses, for NiTi samples subjected to fatigue loading. In the samples analyzed in this work, such a drop in local stresses, due to plastic deformation as shown in the accumulation of irrecoverable strains, will result in the observed local degradation in transformation strains as highlighted using DIC and eventually lead to the total incremental drop in global transformation strains with continued cyclic loading.

If the incremental accumulation of irrecoverable strains, dominated by plasticity as discussed above, was the source behind the drop in transformation strains, then dropping the stress back to 150 MPa should stop, or significantly slow, the incremental drop in transformation strains. To

confirm this, the sample used in the incremental experiment was subjected to additional cycling starting from the lowest stress level (*i.e.,* 150 MPa) and back to highest stress of 250 MPa. The transformation strain response of three cycles at each stress level discussed in Fig. 11 confirms that dropping the stress back to 150 MPa resulted in a more stable response with no obvious degradation in ε_{trans} over three loading cycles. Increasing the stress back to 250 MPa, has triggered back the incremental degradation in ε_{trans} as clear accumulation of irrecoverable strains takes place at this stress level.

4.3. The Initial Increase in Transformation Strains and Localization Effects

The other outstanding issue observed in ε_{trans} during the first few fatigue cycles, particularly at 150 and 200 MPa, is the reason behind the initial increase in the magnitude of the transformation strains. The driving force for such an increase in the globally measured magnitudes could be a local increase in the stress field. With higher local stresses, the resulting local transformation strains are expected to rise. Another possibility is a homogenization process where more regions start to contribute to transformation and thus result in a total increase in global transformation strains. With full field and local strain measurements using DIC, homogenization can by quantified using the full field standard deviation and an increased level of strain localizations can be visually observed using the contour plots. To investigate these aspects due to both global stress increase and cyclic loading, we focus the discussion on the experiment with incremental stress increase (15 cycles at each stress level, all on the same sample). The full field ε_{trans} contour plots in Fig. 7 shows a local increase in the level of transformation strains in the same spatial regions with global stress increase. Observing some regions that persistently did not contribute to the transformation strains (notice blue region in the contour plots) and the fact that total increase in transformation strains took place in the same

local regions provides evidence that no homogenization of the transformation strain field or redistribution of the transformation strains occurred with increasing the stress level (notice the increase in the ε_{trans} field standard deviation shown in the strain histograms in Fig. 7d). The use of the standard deviation of the transformation strain field provides useful quantitative means to assess changes in the local ε_{trans}. To evaluate the changes during thermal cycling at the constant stress level, we focus on the results presented in Fig. 9 (150 MPa). The strain histograms show a clear increase in transformation strains from cycle 2 to 5 (note that at this low stress level, there is insignificant accumulation of irrecoverable strains at the considered number of cycles, thus the transformation and total strains are equivalent). By focusing on the local strains, the line scan shown in Fig. 9c (marked on the contour plot) reveals that the increase in the transformation strains is taking place in the same spatial regions with continued loading. The region with low strain experienced insignificant change. The contour plots in Fig. 9d – 9g provides additional evidence for local increase in ε_{trans} in the same spatial regions with cyclic loading. Notice that the rate of increase is high initially and diminishes with continued cycling. These local changes will result in an increased level of deformation heterogeneity and can be tracked across the entire region of interest by monitoring the evolution of the transformation strain field standard deviation. This analysis (Fig. 8b) for the considered stress level reveals a clear increase in standard deviation over the first 5 cycles followed by stabilized response. The trend is consistent with the conclusions made by observing the line scan and contour plots over a relatively small region in Fig. 9.

The previous analysis highlights that the global increase in transformation strains in the first few cycles of fatigue loading was a result of local increases in transformation strains rather than a spread or homogenization process of the transformation strains field. This suggests that

local stress increase plays a major role in the observed response. Measurement of the local stress field and its evolution in fatigue can be provided using neutron diffraction. Several researchers have conducted such studies in NiTi and NiTiHf where they reported local increases in stress induced by changes in defect density [18, 20], particularly in the first few cycles of fatigue loading. Local increase in the transformation strains indirectly suggests that a similar increase in the local stress is the source behind the observed cyclic increase in ε_{trans} in the first few cycles of fatigue loading.

5. Conclusions

The work supports the following conclusions:

1- The transformation strains for $Ni_{50.3}Ti_{25}Hf_{24.7}$ are visualized by separating the total strain and plastic strain components. The transformation strains increase substantially upon increase in stress from 150 to 250 MPa and exhibit a transient behavior under temperature cycling. After a rapid increase with cycles, the transformation strain magnitude stabilizes before it undergoes a gradual reduction with continued cycling. The rate of transformation strain degradation was strongly dependent on the stress level and the accumulation of irrecoverable strains.

2- By conducting isobaric experiments with incremental stress increase on the same sample, we showed a clear correlation between global stress increase, the accumulation of irrecoverable strains, and eventually the rate of transformation strain degradation with cycling. Although the degradation in transformation strain magnitudes can be a result of plastic deformation and/or the accumulation of residual martensite/austenite, the results and analysis in this work suggest a major role of plasticity.

3- By analyzing the distribution of strain using digital image correlation, it was possible to show that localization of strain intensified with cycling in the first few fatigue cycles. The same localized regions underwent forward and reverse transformation while substantial non-transforming domains exist. By evaluating the strains in a statistical fashion, it was shown that the global increase in transformation strains in the first few cycles of fatigue loading was a result of local increases in transformation strains rather than a spread or homogenization process of the transformation strains field. Therefore it is inferred that local stress increase plays a major role in the observed response (*e.g.*, increase in defect density resulting in higher local stresses).

4- In addition to the changes in transformation strains, the study found that hysteresis levels and transformation temperatures evolve slightly with stress. Considering the high subjected temperatures, it was remarkable that the temperature hysteresis was below 50 ºC and that transformation strains exceeded 8 % in tension. Further heat treatments could change the microstructure and hence the local strain response and will be the subject for future studies.

Acknowledgements

The work is supported by a National Science Foundation grant NSF CMMI- 1333884 which is gratefully acknowledged. The authors acknowledge the assistance of Prof. Yury Chumlyakov (Tomsk State University) for his assistance. The corresponding author would like to acknowledge the partial financial support from the American University of Sharjah through the Office of Research and Graduate Studies (FRG16-T-16).

References:

[1] H. Sehitoglu, L. Patriarca, and Y. Wu, "Shape memory strains and temperatures in the extreme," *Current Opinion in Solid State and Materials Science,* 2016 2016.

[2] J. Wang and H. Sehitoglu, "Modelling of martensite slip and twinning in NiTiHf shape memory alloys," *Philosophical Magazine,* vol. 94, no. 20, pp. 2297-2317, 2014.

[3] J. Ma, I. Karaman, and R. D. Noebe, "High temperature shape memory alloys," *International Materials Reviews,* vol. 55, no. 5, pp. 257-315, 2010.
[4] H. Sehitoglu *et al.*, "Compressive response of NiTi single crystals," *Acta Materialia,* vol. 48, no. 13, pp. 3311-3326, 2000.
[5] Y. Wu *et al.*, "Shape Memory Response of Polycrystalline NiTi12.5Hf Alloy: Transformation at Small Scales," *Shape Memory and Superelasticity,* journal article vol. 1, no. 3, pp. 387-397, 2015.
[6] G. S. Bigelow, A. Garg, S. A. Padula Ii, D. J. Gaydosh, and R. D. Noebe, "Load-biased shape-memory and superelastic properties of a precipitation strengthened high-temperature Ni50.3Ti29.7Hf20 alloy," *Scripta Materialia,* vol. 64, no. 8, pp. 725-728, 2011.
[7] H. E. Karaca *et al.*, "Effects of nanoprecipitation on the shape memory and material properties of an Ni-rich NiTiHf high temperature shape memory alloy," *Acta Materialia,* vol. 61, no. 19, pp. 7422-7431, 2013.
[8] A. P. Stebner *et al.*, "Transformation strains and temperatures of a nickel–titanium–hafnium high temperature shape memory alloy," *Acta Materialia,* vol. 76, pp. 40-53, 2014.
[9] S. M. Saghaian, H. E. Karaca, M. Souri, A. S. Turabi, and R. D. Noebe, "Tensile shape memory behavior of Ni50.3Ti29.7Hf20 high temperature shape memory alloys," *Materials & Design,* vol. 101, pp. 340-345, 2016.
[10] O. Benafan, R. D. Noebe, S. A. Padula, and R. Vaidyanathan, "Microstructural Response During Isothermal and Isobaric Loading of a Precipitation-Strengthened Ni-29.7Ti-20Hf High-Temperature Shape Memory Alloy," *Metallurgical and Materials Transactions A,* journal article vol. 43, no. 12, pp. 4539-4552, 2012.
[11] O. Benafan *et al.*, "Mechanical and functional behavior of a Ni-rich Ni50.3Ti29.7Hf20 high temperature shape memory alloy," *Intermetallics,* vol. 50, pp. 94-107, 2014.
[12] O. Benafan *et al.*, "Constant-Strain Thermal Cycling of a Ni50.3Ti29.7Hf20 High-Temperature Shape Memory Alloy," *Shape Memory and Superelasticity,* journal article vol. 2, no. 2, pp. 218-227, 2016.
[13] R. Santamarta *et al.*, "TEM study of structural and microstructural characteristics of a precipitate phase in Ni-rich Ni–Ti–Hf and Ni–Ti–Zr shape memory alloys," *Acta Materialia,* vol. 61, no. 16, pp. 6191-6206, 2013.
[14] K. Gall, H. Sehitoglu, Y. I. Chumlyakov, I. V. Kireeva, and H. J. Maier, "The Influence of Aging on Critical Transformation Stress Levels and Martensite Start Temperatures in NiTi: Part I—Aged Microstructure and Micro-Mechanical Modeling," *Journal of Engineering Materials and Technology,* vol. 121, no. 1, pp. 19-27, 1999.
[15] F. Yang *et al.*, "Structure analysis of a precipitate phase in an Ni-rich high-temperature NiTiHf shape memory alloy," *Acta Materialia,* vol. 61, no. 9, pp. 3335-3346, 2013.
[16] D. R. Coughlin, "Characterization of Stoichiometric and Aging Effects on NiTiHf High Temperature

Shape Memory Alloys," Doctor of Philosophy, Materials Science and Engineering, The Ohio State University, 2013.
[17] A. EVIRGEN, F. BASNER, I. KARAMAN, R. D. NOEBE, J. PONS, and R. SANTAMARTA, "EFFECT OF AGING ON THE MARTENSITIC TRANSFORMATION CHARACTERISTICS OF A Ni-RICH NiTiHf HIGH TEMPERATURE SHAPE MEMORY ALLOY," *Functional Materials Letters,* vol. 05, no. 04, p. 1250038, 2012.
[18] O. Benafan, "Deformation And Phase Transformation Processes In Polycrystalline Niti And Nitihf High Temperature Shape Memory Alloys " Doctor of Philosophy, Department of Mechanical, Materials and Aerospace Engineering, University of Central Florida, 2012.

[19] B. Kockar, I. Karaman, J. I. Kim, and Y. Chumlyakov, "A method to enhance cyclic reversibility of NiTiHf high temperature shape memory alloys," *Scripta Materialia,* vol. 54, no. 12, pp. 2203-2208, 2006.
[20] P. Sedmák, P. Šittner, J. Pilch, and C. Curfs, "Instability of cyclic superelastic deformation of NiTi investigated by synchrotron X-ray diffraction," *Acta Materialia,* vol. 94, pp. 257-270, 2015.
[21] L. Patriarca, H. Sehitoglu, E. Y. Panchenko, and Y. I. Chumlyakov, "High-temperature functional behavior of single crystal Ni51.2Ti23.4Hf25.4 shape memory alloy," *Acta Materialia,* vol. 106, pp. 333-343, 2016.
[22] L. Patriarca, Y. Wu, H. Sehitoglu, and Y. I. Chumlyakov, "High temperature shape memory behavior of Ni50.3Ti25Hf24.7 single crystals," *Scripta Materialia,* vol. 115, pp. 133-136, 2016.
[23] R. F. Hamilton, H. Sehitoglu, Y. Chumlyakov, and H. J. Maier, "Stress dependence of the hysteresis in single crystal NiTi alloys," *Acta Materialia,* vol. 52, no. 11, pp. 3383-3402, 2004.

Abuzaid, W., & Sehitoglu, H. (2017). Functional fatigue of Ni 50.3 Ti 25 Hf 24.7–Heterogeneities and evolution of local transformation strains. Materials Science and Engineering: A.
https://doi.org/10.1016/j.msea.2017.04.097